APPLIED MATERIALS AND TECHNOLOGY

Jamt.ejournal.unri.ac.id

Research Article

Assessing immobilization matrices for nuclear effluent treatment: Cs case study

Costa-Silva, D. L.[1a], Fungaro, D. A.[1b], Las Casas, A.[1c], Silva P. S. C.[1d], Vicente, R.[1c], Araujo, M. S.[1a], Izidoro, J. C.[1b], Mello-Castanho, S.[*1a]

ABSTRACT: The immobilization processes for nuclear waste have gained significant attention from the scientific community due to the growing global activity in the nuclear industry. Although these processes have been studied and applied since the mid-20th century, many questions remain that require further in-depth research, including the immobilization itself and the deposition of wasteforms in repositories designed to safeguard against future exposure. In this study, highly phase-pure zeolite A was synthesized via hydrothermal processing of coal fly ash from a Brazilian thermal power plant and loaded with Cs to evaluate thermal stability, structure, and immobilization in Nb-aluminoborosilicate and geopolymer matrices. Cs adsorption, confirmed by XRD peak intensity and Raman band changes, showed a 26 wt.% incorporation (INAA) after 24-hour sorption using simulated CsCl solution, a notable result given the fly ash impurities. The zeolite structure remained stable during the heating up to 960 °C, forming water-insoluble phases (pollucite and cesium aluminum oxide) right after structural collapse between 700 °C and 900 °C. Up to 40 wt.% of Cs-loaded waste was incorporated into a monolithic ceramic via thermal treatment of Nb-aluminoborosilicate glass and zeolite A at 900 °C for 2 hours, yielding a dense body (2.4 g/cm^3) with low porosity (3.6%) and water absorption (1.63%). In contrast, raw Cs-loaded zeolite A showed high porosity (48%), water absorption (33%), and low density (1.44 g/cm^3). Crystalline Cs phases formed at lower temperatures (900 °C) due to the devitrification nature of the glass. Geopolymer matrices immobilizing Cs-loaded zeolite exhibited water leachability comparable to similar materials, meeting nuclear waste disposal requirements.

Keywords: *Coal fly ash, radioactive cesium, geopolymers, niobium aluminoborosilicate glasses, Cs-loaded zeolite A*

1. INTRODUCTION

It was during the early 1950s that the risks associated with radioactive waste (RW) first became known to the scientific community. Following the tragic nuclear bombings of Hiroshima and Nagasaki in 1945, as well as nuclear accidents such as Chernobyl (1986) and Fukushima (2011), and with the rise in nuclear activities through the late 20th century, the potential dangers of these activities became widely recognized by the global population [1]. Given the environmental consequences of improper RW disposal, the need for effective radiological shielding and the stable, long-term management of such highly hazardous materials has become an urgent priority [2].

In addition to decades of nuclear activities and the accumulation of high-level radioactive waste (HLW) at nuclear power facilities, these wastes are currently stored in temporary facilities [3]. After many years of research into potential solutions, deep geological repositories have been identified as the safest option. However, to date, only one such repository is in advanced construction in Olkiluoto, Finland, which is expected to become the world's first operational nuclear waste repository within the next few years [4]. Nonetheless, the construction of these geological sites requires substantial financial investment and multidisciplinary expertise and represents only a partial solution to RW management.

Affiliation
[1]Instituto de Pesquisas Energéticas e Nucleares, IPEN/CNEN Av. Prof. Lineu Prestes, 2242 - Cidade Universitária - CEP 05508-000 São Paulo - SP - Brasil
[a]Centro de Ciência e Tecnologia de Materiais (CECTM)
[b]Centro de Química e Meio Ambiente (CEQMA)
[c]Serviço de Gestão de Rejeitos Radioativos (SEGRR)
[d]Centro do Reator de Pesquisa (CERPQ)

***Correspondence**
Email: srmello@ipen.br

ORCID
Costa-Silva, D. L: 0000-0001-5852-637X
Fungaro, D. A: 0000-0003-1618-0264
Silva P. S. C: 0000-0002-9351-9201
Araujo, M. S: 0000-0002-0519-6263
Izidoro, J. C: 0000-0002-3466-5196
Mello-Castanho, S: 0000-0002-0155-9100

Received: November 15, 2024
Revised: December 18, 2024
Accepted: December 20, 2024

How to cite: Lopes Costa e Silva, D., Alves Fungaro, D., Las Casas, A., Sergio Cardoso da Silva, P., Vicente, R., Silva de Araujo, M., Carvalho Izidoro, J., & Mello-Castanho, S. (2025). Assessing immobilization matrices for nuclear effluent treatment: Cs case study. Journal of Applied Materials and Technology, 6(1), 1–13. https://doi.org/10.31258/Jamt.6.1.1-13.

HLW can only be stored in these facilities after undergoing appropriate treatment and processing to create stable, chemically inert, and radiation-resistant forms [5].

In the search for materials that meet these stringent specifications, ceramics, glasses, and glass-ceramics have proven to be the most suitable matrices for HLW immobilization. These materials offer excellent chemical durability, impermeability to liquids, and resistance to radiation-essential properties for long-term disposal and protection against future exposure [6].

Among the major fission products contained in HLW, the isotope ^{137}Cs poses a significant threat to human health due to its high activity and emission of beta and gamma radiation. With a half-life of 30.2 years, ^{137}Cs is particularly hazardous as it can easily disperse into the environment, facilitated by its high solubility in water and ease of transport [7].

One effective approach for mitigating environmental contamination by radionuclides is the adsorption method, which demonstrates excellent performance in the selective and safe removal of radionuclides from contaminated water. This method is characterized by operational simplicity, adaptability to low-contamination effluents, and the availability of various low-cost adsorbents, making it suitable for both continuous and batch processes [8].

Zeolites, also known as "molecular sieves," are characterized by high ion-exchange capacities (IEC), excellent selectivity for specific elements, and good thermal and radiation stability [9]. Cationic radioisotopes present in aqueous effluents can be removed through ion exchange with Na^+ ions [10]. Among various types of zeolites, Na-A (Linde Type A - LTA) zeolite has proven to be highly efficient in removing cesium isotopes ($^{134}Cs^+$, $^{135}Cs^+$, $^{137}Cs^+$), $^{90}Sr^{2+}$, and $^{60}Co^{2+}$ from aqueous solutions [11–13]. Moreover, the ability to synthesize Type A zeolite from coal fly ash using a low-cost, open-system hydrothermal process makes it an attractive choice as an adsorbent material derived from industrial waste. However, for long-term disposal, ^{137}Cs-loaded zeolites are not stable in the presence of groundwater, as they may degrade and release the radionuclide. To address this limitation, ion-exchanged zeolites have been incorporated into dense matrices such as cement blends, glasses, and geopolymers, ensuring improved stability for safe waste immobilization [14–17].

The immobilization of HLW in glass and glass-ceramic matrices is widely regarded as one of the most suitable methods for its safe management [18]. Countries such as the UK, France, Russia, the USA, China, Germany, and Japan have adopted the use of glass matrices, primarily alkaline borosilicate glasses and phosphate glasses, with compositions tailored to the solubility of the waste elements in the glassy phase [19]. However, the potential infiltration of groundwater into deep geological repositories presents a risk of environmental contamination. Depending on their chemical resistance, glass matrices containing immobilized radionuclides may undergo dissolution due to hydrolytic attack [20,21]. In this context, glass-ceramics have garnered significant attention from scientists, as these materials offer improved mechanical properties and enhanced thermal stability compared to traditional RW glasses. These advantages make glass-ceramics a promising alternative for HLW immobilization.

Geopolymers (GP) are inorganic polymers with a robust chemical structure, formed through the polycondensation of mineral materials containing aluminosilicates [22]. They are synthesized by reacting aluminosilicate materials with an alkaline activator, typically a concentrated solution of hydroxides, silicates, carbonates, or sulfates. Geopolymers exhibit excellent resistance to high temperatures, thermal shocks, chemical corrosion, and abrasion [23,24].

In the nuclear field, geopolymers have been utilized in the Czech Republic and Slovakia since 2003 to immobilize evaporator concentrates, ion exchange resins, and radioactive liquid waste containing ^{137}Cs [25]. Furthermore, geopolymers can be synthesized using sewage treatment plant sludges, a byproduct of industrial and urban activities [26].

In this study, zeolite A was produced through hydrothermal synthesis using coal fly ash as the silicon source and applied as an ion-exchange medium to capture cesium from a CsCl (non-radioactive) aqueous solution. This approach aims to simulate the treatment of ^{137}Cs-rich effluents within two distinct matrices: Nb-aluminoborosilicate glass and geopolymer. The high purity, crystallinity, and homogeneity of the zeolitic material make it an excellent intermediate step for immobilizing radioactive cesium.

While the incorporation of Cs-loaded zeolitic materials into geopolymer matrices has been previously studied [22,26], this work investigates the leaching behavior of cesium in a geopolymer matrix, as detected through a nuclear technique. For the Nb-aluminoborosilicate matrix, this study evaluates the densification of thermally treated waste forms, exploring the benefits of this new nuclear glass composition [27]. Aligned with the principles of the circular economy and the Sustainable Development Goals (SDGs), particularly SDG 12, the zeolite samples used in this research were synthesized from coal fly ash [28–30].

2. METHODS

2.1. Synthesis of zeolite A and sorption experiment.

The zeolite samples were prepared following the procedure outlined in previous studies [30,31], using coal fly ash (CFA) sourced from the Jorge Lacerda thermal power plant in Santa Catarina (SC), Brazil. The chemical composition of the CFA, shown in Table 1, consists predominantly of SiO_2 and Al_2O_3, with a suitable Si/Al ratio for synthesizing zeolitic materials. Additional constituents, such as a relatively high CaO content and minor amounts of Fe_2O_3, K_2O, TiO_2, MgO, and SO_3, are characteristic of this CFA and are typically observed in Class C coal fly ashes [28,31,32].

Table 1. Chemical composition (wt.%) of the coal fly ash.

Component	CFA
SiO2	48.8
Al_2O_3	25.0
CaO	11.9
Fe_2O_3	6.1
K_2O	2.9
TiO_2	1.4
MgO	1.9
SO_3	1.6
Other	0.4
SiO_2/Al_2O_3	1.95

The CFA and pulverized NaOH were homogenized in a 1:1.2 weight ratio in a crucible, and the mixture was then melted in a furnace at 550°C for 2 hours to ensure the complete dissolution of quartz (SiO_2) from the CFA. After cooling to room temperature, the mixture was transferred to a PTFE beaker containing 0.150 L of deionized water and $NaAlO_2$ (50-60% Al_2O_3, Riedel-de Haen) to adjust the Si/Al ratio. The mixture was heated in an oven at 100°C for 3 hours to perform the hydrothermal synthesis, followed by filtration and drying in an oven at 105°C for 16 hours. The sorption experiments were carried out according to the procedure described in the literature [33]. The synthesized zeolite A and CsCl (non-radioactive, Sigma-Aldrich 99.9%) were mixed in a 1:1 mass ratio and added to 0.5 L of deionized water. The mixture was stirred for 24 hours, filtered, and then dried in an oven for 16 hours. As mentioned earlier, this procedure was designed to simulate the capture of ^{137}Cs from liquid radioactive wastes.

2.2. Composite materials class 1 (Nb-Aluminoborosilicate glasses + Cs-loadeed zeolite A, G6ZCs). The nominal (wt.%) composition of the glass sample used in this work is $42SiO_2$-$8B_2O_3$-$23Na_2O$-$18CaO$-K_2O-$2Al_2O_3$-$6Nb_2O_5$. The parent glass composition (without Nb) has demonstrated excellent retention (up to 40 wt.%) of galvanic waste within the glass network structure [34,35], and it has been thermally and structurally evaluated in our previous studies with Nb additions [27,36]. This specific composition was selected for the immobilization process due to its favorable thermal stability and reduced melt viscosity, both of which are enhanced by the inclusion of up to 6.0 wt.% Nb, facilitating the incorporation of zeolitic materials. The G6ZCs pellets were prepared in duplicate by homogenizing a mixture of Nb-aluminoborosilicate glass and Cs-loaded zeolite A particles (0.4 to 0.6 μm) in a 2:3 weight ratio, using a ball milling system for 24 hours. The resulting mixture was then subjected to uniaxial pressing (1 Ton/cm^2) at room temperature using a powder pellet press die. The pellets were heat-treated at 900°C for 2 hours in atmospheric air, followed by slow cooling to room temperature inside the furnace.

2.3. Composite materials class 2 (Geopolymer + Cs-loaded zeolite, ZG). The analysis of the precursors involved using materials with high silica (SiO_2) and alumina (Al_2O_3) content, such as metakaolin. A solution of sodium hydroxide (NaOH) and sodium silicate (Na_2SiO_3), both at 8 mol/L, were used as alkaline activators. Chemical analyses were performed to determine the contents of SiO_2, Al_2O_3, and Na_2O, and to calculate the molar ratios (SiO_2/Al_2O_3 and Na_2O/Al_2O_3). The zeolite was previously saturated with a ^{137}Cs radioactive tracer, using a 12.7 g/L CsCl solution, with the pH adjusted to 7 and spiked with 311 becquerels of ^{137}Cs activity. In preparing the mixture, the amounts of each material were adjusted to achieve the desired molar ratios, typically ranging between 3 and 4 for SiO_2/Al_2O_3 and between 0.8 and 1.2 for Na_2O/Al_2O_3. Geopolymer production was conducted in duplicate and involved mixing the dry materials with alkaline activators, adding the calculated amount of activator solution to achieve the desired Na_2O/Al_2O_3 molar ratio, and stirring until a homogeneous paste was formed. This paste was then molded into shapes and cured for 6 hours at 60 °C in an oven, followed by curing in air at room temperature (around 25 °C) and room humidity to allow the geopolymer structure to develop. To optimize the mechanical properties and durability of the geopolymer for specific applications, the proportions were adjusted, and accelerated curing conditions were applied.

ASTM C1308-21 [37] was conducted to investigate the leaching behavior of cesium in the solidified zeolite/geopolymer (ZG) specimens. The samples were placed in leaching vessels containing 147 mL of deionized water, ensuring that all sides were in contact with the leachant. The leachate was replaced with fresh water at 2 hours, 7 hours, 1 day, and then daily until the 11th day. The leaching behavior of cesium from the ZG specimens was evaluated based on the leaching rate (LR) and the cumulative fraction leached (CFL). The LR_n is defined as the amount of a constituent of a solid material that is leached during a given time interval, n, during the leaching test. The LR of ^{137}Cs from the ZG specimens was calculated using the following equation:

$$LR = \frac{\sum_n a_n}{A_o} \cdot \left(\frac{V}{S}\right) \cdot \left(\frac{1}{t}\right) \quad (1)$$

where a_n is the amount, in Bq, of the nuclide released from the specimen during the leaching interval n, A_0 is the total amount of the nuclide in the specimen (Bq), V is the geometric volume of the specimen (cm^3), S is the geometric surface area of the specimen (cm^2), and t (day) is the leaching time measured from the beginning of the leaching test [38].

2.4. Characterization. X-ray diffractometry was performed using a Rigaku SmartLab instrument with Cu-Kα radiation, in theta-2theta configuration, at a scan rate of 0.05°/s. The structural illustrations were generated using Vesta™ [39], based on CIF files from the Crystallographic Open Database (COD) of the identified phases. Chemical analyses were conducted with an Energy Dispersive X-ray Fluorescence Spectrometer (ED-XRF), Shimadzu EDX 720, using Ti-U/Na-Sc analytes. Differential Thermal Analysis (DTA) of the Cs-loaded synthesized zeolite material was carried out using a Netzsch DSC/DTA 404F3 instrument at a heating rate of 10°C/min in synthetic air up to 1300°C. Fourier-Transform Infrared Spectroscopy (FTIR) was performed using a Thermo Nicolet Nexus 670 spectrometer, in ambient atmosphere, with a spectral resolution of 0.125 cm^{-1} using the KBr technique. Raman spectra were collected on powder samples with a confocal Witec Alpha 300R Raman microscope, using a 532 nm (Ar^+ green laser) at 45 mW. Scanning Electron Microscopy (SEM) of the raw zeolite sample was conducted using a Quanta FEG 650 FEI microscope at 15 kV. For the Cs-loaded zeolite sample, a Jeol JSM-6701F instrument operating at 6 kV was used. Density, water absorption (%), and porosities were determined according to ASTM C1285-02 [40].

The concentration of Cs was assessed using Instrumental Neutron Activation Analysis (INAA). Due to the high concentration and large cross-section (30.1 barns) of Cs, it was necessary to irradiate a small sample mass to keep the dead time of the counting system at an acceptable level (e.g., below 10%). Therefore, approximately 5 mg of samples were weighed for analysis. A paper sheet, onto which a known concentration of Cs standard solution was pipetted and dried under infrared light, was used as the comparator. The samples and paper sheets were sealed in pre-cleaned double polyethylene bags, placed parallel to each other in the irradiation container to receive the same neutron flux, and then sent for irradiation. The samples and comparator were irradiated in the IEA-R1 nuclear research reactor at IPEN (Instituto de Pesquisas Energéticas e Nucleares) for 8 hours under a thermal neutron flux of 10^{12} cm^{-2} s^{-1}. Radionuclide (^{134}Cs) counting was performed via gamma

spectrometry using a high-purity germanium (HPGe) detector from Canberra Industries, with a resolution of 0.88 keV for ^{57}Co and 1.90 keV for ^{60}Co, coupled to a DSA-1000 multichannel analyzer. The ^{134}Cs counting was carried out after a 15-day cooling period, for 2 hours, and spectral analysis was performed using Genie 2000 and CAX software, which allows for the identification of each gamma energy transition. The results are presented as mean values (g/g) for duplicate samples, and error propagation was applied to determine uncertainties. The method's validation was confirmed by analyzing the reference material USGS STM-2, as shown in Table 2.

Table 2. Relative standard deviation (RSD) and relative error (RE) for USGS STM-2 standard material used for INAA analyses.

	USGS STM-2						
rns	Certified		Calculated		RSD(%)	RE(%)	E_n-score
	1.52	±0.06	1.50	±0.08	5	1	0.2

3. RESULTS

3.1. Characteristics of the Cs-loaded waste (Cs-loaded zeolte A). Despite the use of zeolites as adsorbent materials for the selective decontamination of various types of waste, their efficiency depends on crucial characteristics such as crystallinity, purity, and homogeneity, especially when these materials are derived from ashes that may contain a wide variety of contaminants. These characteristics also impact their incorporation into matrices and must therefore be investigated in greater depth.

Figure. 1 shows the XRD patterns of the raw zeolite sample and the Cs-loaded zeolite sample (ZeoACs). Both are identified as phase-pure Na-A type zeolite (JCPDS 43-0142). The absence of peaks related to typical impurities, such as undissolved quartz (SiO_2) particles and mullite ($70Al_2O_3{\cdot}30SiO_2$), which are present in coal fly ash [30,31], suggests that these components were adequately dissolved by NaOH during the melting process (550 °C/2h). This specific Class C coal fly ash, sourced from southern Brazil, is generated by a thermal power plant in which pulverized coal is burned using air entrainment at temperatures between 1200 °C and 1400 °C. Such high temperatures result in ashes with amorphous content and hollow particles, which enhance the alkaline activation and synthesis processes [31]

Figure 2 shows the SEM images of the zeolite sample before (a-b) and after Cs adsorption (c-d). The microstructure of the zeolitic material is predominantly composed of well-crystallized cubic particles exhibiting regular edges and a homogeneous size distribution, ranging from 840 to 869 nm, suggesting a high-quality zeolitic material. Additionally, a small number of particles exhibiting irregular shapes and varying sizes can also be observed, which may indicate the presence of other crystalline phases, undetectable by XRD due to their negligible content [30]. When comparing the aspect and size of particles before (a-b) and after the Cs adsorption (c-d), no differences are observed, suggesting the high stability of the zeolitic material under the sorption experiments.

The FTIR spectra of the raw and ZeoACs samples are shown in Figure. 3. The zeolite exhibits typical bands related to zeolitic materials primarily composed of Si and Al: the band at 464 cm^{-1} is attributed to O-Si-O bending vibrations, and the band at 558 cm^{-1} is complex, attributed to the external stretching modes of the

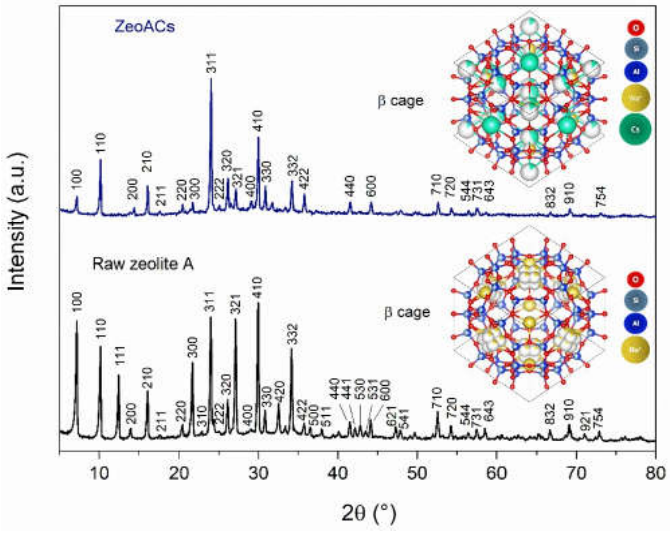

Figure 1. X-ray diffraction (XRD) patterns of raw zeolite A and Cs-loaded zeolite A (ZeoACs), including an illustration of the beta cage (the sodalite fundamental structure) after Na^+ exchange with Cs^+ .

bridges between the tetrahedra (Si-O-Si) and the bending mode of the O-Si-O bonds. The band at 667 cm^{-1} is attributed to the symmetric stretching of the Si-O-Al bridge bonds, while the band at 1006 cm^{-1} corresponds to the asymmetric stretching vibrations of the Si-O(Si) and Si-O(Al) bridge bonds [41,42]. The bands at 1651 cm^{-1} and 3420 cm^{-1} are attributed to the asymmetric and symmetric stretching modes of O-H functional groups, respectively [43,44].

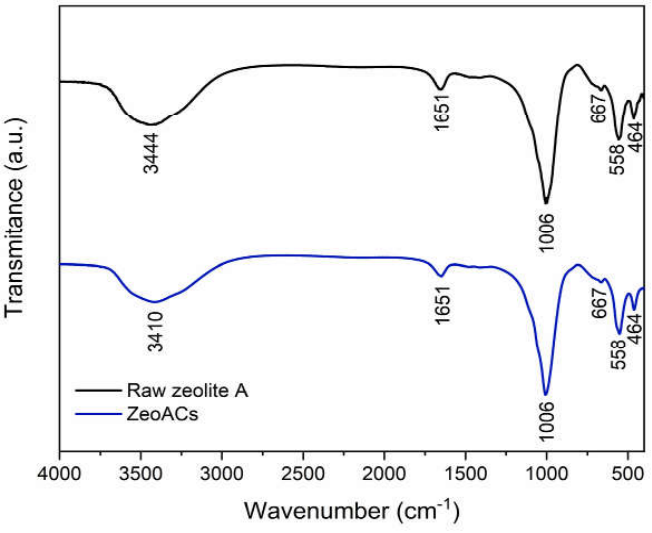

Figure 3. Fourier-transform infrared spectra (FT-IR) of the zeolite A before and after the adsorption experiment.

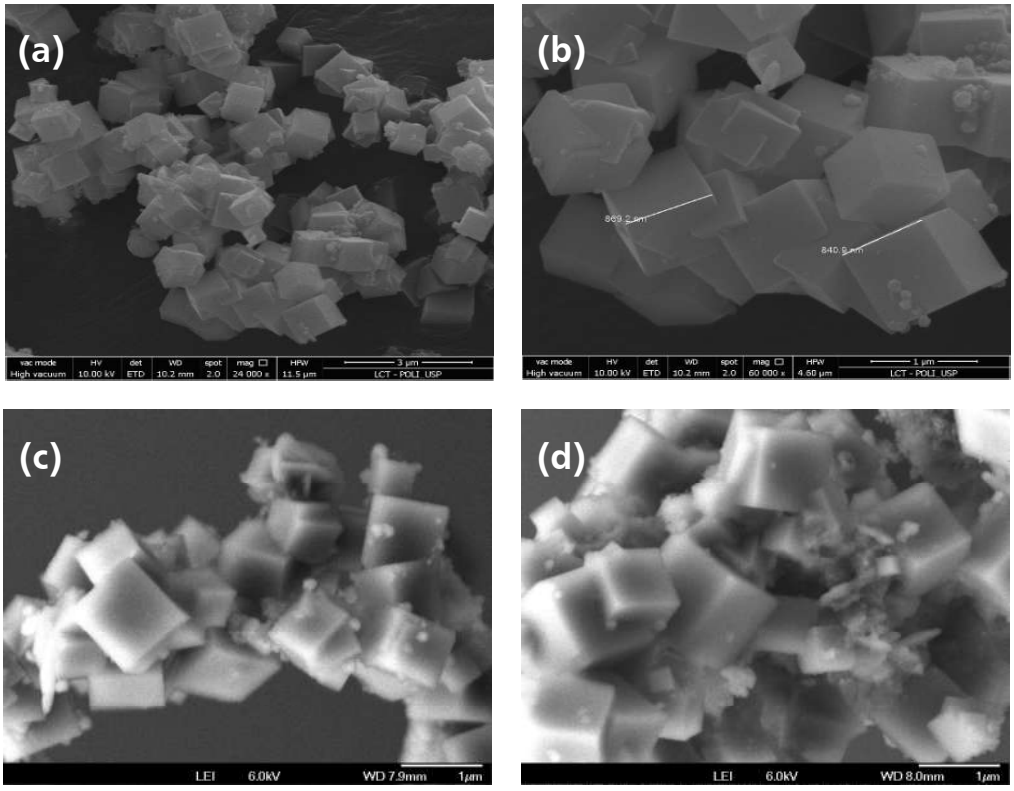

Figure 2. Scanning electron microscope images (SEM) showing the cubic structure of: (a-b) raw zeolite A and (c-d) Cs-loaded zeolite A.

Figure. 4 shows the room temperature Raman spectra of the raw and ZeoACs samples. The most intense band, at 495 cm^{-1}, is attributed to the bending mode of Si-O-Al 4-membered rings (Si, Al) [45]. The bands at 338 cm^{-1} and 413 cm^{-1} are related to the bending mode of the 6-membered Si-O-Al rings [46]. The bands at 980 cm^{-1}, 1044 cm^{-1}, and 1100 cm^{-1} are attributed to the asymmetric stretching of T-O (T = Si, Al) [46,47]. The bands in the region between 600 and 900 cm^{-1} are related to the symmetric stretching of T-O type bonds [48]. The band at 702 cm^{-1} is characteristic of A-type zeolites and is attributed to the 4-membered double rings, which join each sodalite cell (β cell) [45–49].

The raw zeolitic material was chemically evaluated by energy dispersive X-ray fluorescence spectroscopy (ED-XRF), while the ZeoACs zeolite was analyzed for Cs content using instrumental neutron activation analysis (INAA). The results are shown in Table 3. The raw zeolite is primarily composed of SiO_2, Al_2O_3, and Na_2O, particularly in this case where the zeolite was synthesized through the alkaline dissolution of quartz (SiO_2) from coal fly ash using NaOH. Other constituents, such as Fe_2O_3, CaO, and TiO_2, are also present as exchangeable cations, reflecting the specific composition of this coal fly ash (see Table 1). The SiO_2/Al_2O_3 mass ratio is 1.3, and the calculated Si/Al molar ratio is 2.3. The Cs-loaded zeolite was able to incorporate 26 wt.% Cs after the sorption experiment.

When loaded with radioactive cesium (^{134}Cs, ^{137}Cs), zeolitic materials may be subjected to elevated temperatures due to radioactive decay [50]. To investigate the thermal properties of the Cs-loaded zeolite, such as phase transformations and weight loss during heating, differential thermal analysis (DTA) and thermogravimetric analysis (TGA) were conducted, and the results are shown in Figure. 5. Up to 100 °C, the ZeoACs material exhibits an endothermic deviation in the DTA curve, marked by a 5% weight loss (TGA), with peaks at 34.46 °C and 96.99 °C (DTG). As the temperature increases, weight loss continues (TGA), and the DTA curve exhibits pronounced exothermic deviations with two maximum peaks (around 850 °C and 960 °C), indicating heat-induced phase transformations. The total mass loss at 950 °C is 15.63%.

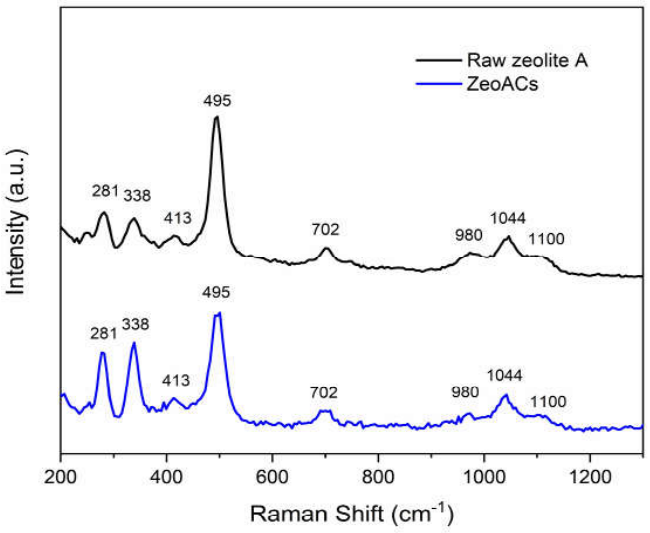

Figure 4. Raman spectra of the zeolite samples before (raw zeolite) and after the adsorption experiment (ZeoACs).

Table 3. Chemical composition (ED-EXF) of the CFA Na-A zeolite material (wt.%) before the sorption experiment using a CsCl aqueous solution, and Cs content (obtain by INAA) after the sorptionexperiment.

Component (wt.%)	Raw zeolite	ZeoACs
SiO_2	41.31	
Al_2O_3	34.76	
^{134}Cs (g/g)	-	0.26
Na_2O	11.94	
CaO	5.64	
Fe2O3	4.30	
TiO2	0.95	
Other	1.1	

The thermal events exhibited by the ZeoACs sample during heating in the DTA results (Figure. 5) were evaluated up to 1000 °C through XRD analysis of heat-treated samples, and the XRD results are shown in Figure. 6. The first transformation of the material, occurring around 845 °C, was found to be related to an amorphous phase coexisting with remaining Na-A zeolite crystals (JCPDS 43-0142), as well as other crystalline phases involving the adsorbed Cs: Pollucite (JCPDS 28-407), Cesium Aluminum Oxide (JCPDS 23-882), Nepheline (JCPDS 35-424), and Hematite (JCPDS 85-987).

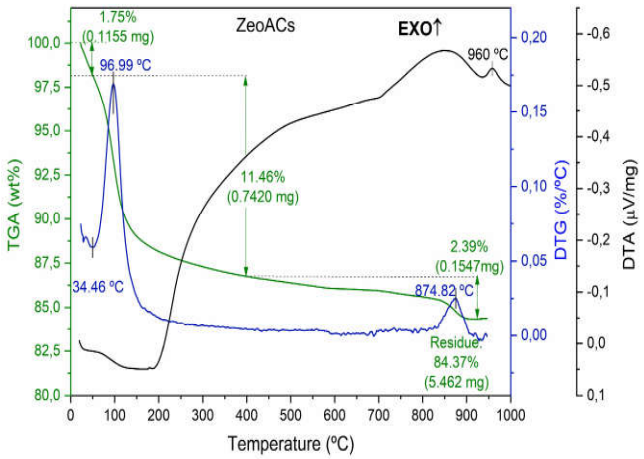

Figure 5. Differential and gravimetric thermal analyzes (DTA, TGA) of the Cs-loaded zeolite sample (ZeoACs), at 10°C.min^{-1} under synthetic atmosphere.

3.2. Examples of hosts for the incorporation of Cs-loaded zeolite: Nb-borosilicate glass and geopolymer matrices. Figure. 7 shows the SEM images of the surface of the heat-treated samples (900 °C/2h): ZeoACs (Cs-loaded zeolite) (column a) and G6ZCs (glass + Cs-loaded zeolite) (column b), each presented with x400 and x150 magnifications. It can be observed that the ZeoACs sample exhibits a porous surface with microcracks. In contrast, the G6ZCs sample has a well-condensed surface with an absence of microcracks and a significantly lower pore concentration.

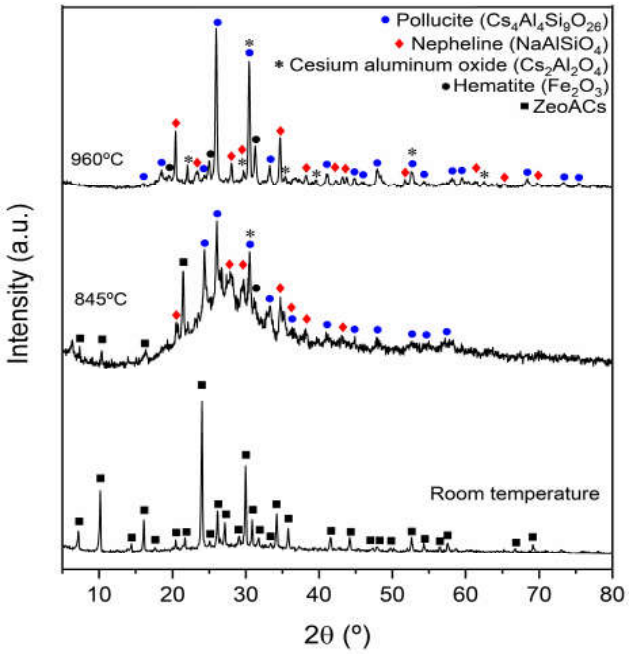

Figure 6. X-ray diffraction (XRD) patterns of the Cs-loaded zeolite (ZeoACs) heat treated at 845°C and 960°C (DTA exothermic peaks), compared to room temperature.

Table 4 presents the cesium concentration in the G6ZCs, as measured by the INAA technique, as well as the data obtained from density calculations according to ASTM C373-88 [40]. It is observed that the ZeoACs exhibited the same Cs content before (Table 3) and after heat treatment (Table 4), while the G6ZCs sample contains 11 wt.% of Cs, which corresponds to the amount present in the pressed mixture. However, in terms of densification, the G6ZCs sample shows higher density, lower water absorption, and reduced porosity compared to the ZeoACs sample.

Table 4. Cs concentration (INAA technique), bulk density (DBULK), apparent porosity (PAP), water absorption (H_2O), volume of open pores (VOP), and impervious portions (VIP) of the heat-treated (900°C) G6ZCs and ZeoACs (ASTM C373-88) [40].

Sample	(Gamma Count)	^{134}Cs (g/g)	V_{OP} (cm^3)	V_{IP} (cm^3)	P_{AP} (%)	H_2O (%)	D_{BULK} ($g.cm^{-3}$)
G6ZCs	2.2h	0.11±0.02	0.01	0.17	3.35	1.40	2.39
ZeoACs	2.2h	0.25±0.02	0.05	0.06	48.13	33.4	1.44

A new option for selectively treating radioactive waste streams is presented by using a chemically resistant Nb-aluminoborosilicate glass matrix to immobilize Cs-loaded Na-A zeolites through heat-induced densification into solid waste forms. The glass precursors help stabilize Cs in the aluminosilicate phase at temperatures up to 900 °C, whereas raw Cs-loaded zeolite waste forms require more energy to achieve the density and porosity compatible with the G6ZCs sample, which exposes adsorbed Cs to ion exchange in water.

Figure. 8 (a and b) shows the leaching rate (LR) and cumulative fraction leached (CFL) of the ZG specimens, expressed as a function of time, respectively. The LR can be thought of as

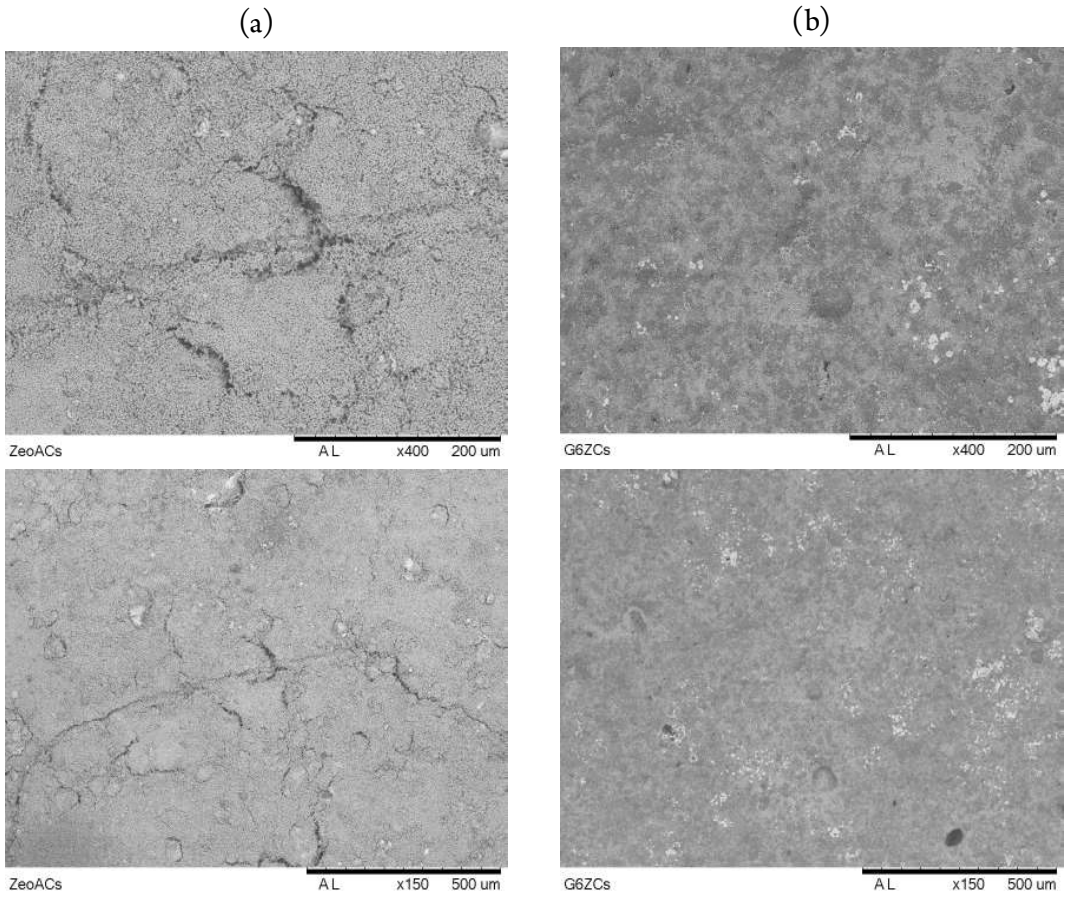

Figure 7. Scanning electron microscope images (SEM) showing the surface of samples after cold pressing and subsequent heat treatment (900 °C): (Column a) ZeoACs and (Column b) G6ZCs

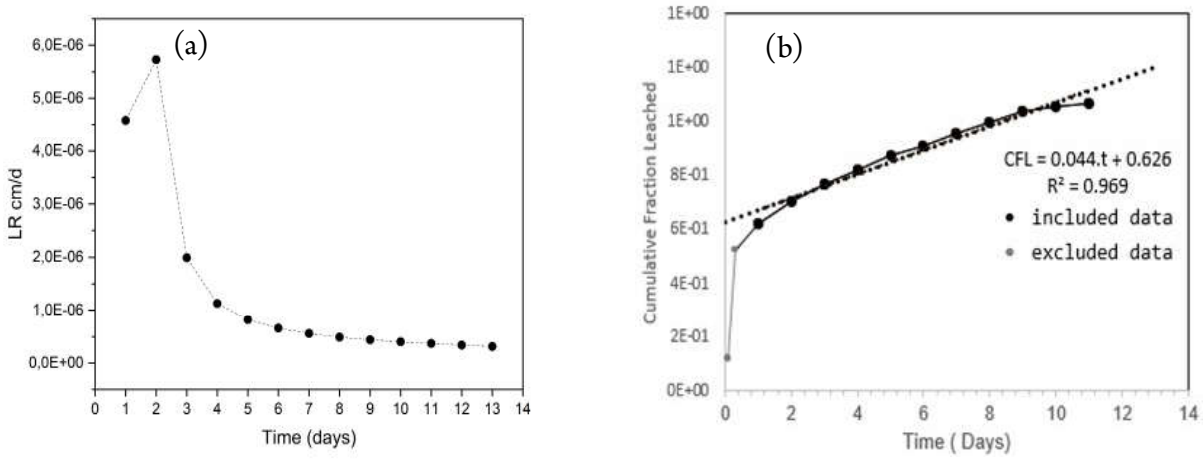

Figure 8. Chemical durability of the Cs-containing geopolymer specimen: (a) leaching rate (cm.d^{-1}) and (b) cumulative fraction leached, showing stabilization around 10^{-6}cm.d^{-1}.

the specimen's volume-to-surface ratio-dependent fraction of the initial activity of the leached constituent, averaged over the leaching time. For cylindrical specimens with a 5 cm diameter and 10 cm height, the LR is numerically equal to the total fraction of the constituent leached during the leach test, divided by the leaching time, expressed in cm.day^{-1}. The cumulative fraction leached (CFLN) is defined as the sum of the fractions of the initial activity (an/A0) of the nuclide contained in the specimen, leached during

leaching intervals, including the Nth interval. The CFLN of 137Cs was calculated by the following equation [17]:

$$CFL_N = \frac{\sum_1^N a_n}{A_0} \quad (2)$$

with the quantities defined by Equation 1, after the initial wash-off period, a rapid increase in the leaching of cesium attached to the surface of the ZG specimens is observed. The LR is primarily controlled by diffusion in a steady-state mode at a constant rate. The LR calculated for the 11th leaching day was 1.23×10-2 cm.d-1. This result is in good agreement with those reported in the literature [17,38,51–54].

4. DISCUSSIONS

An illustration of the fundamental building structure of zeolite A is depicted in Figure. 1. The so-called β cage (or sodalite cage) is composed of alternately interconnected TO_4 tetrahedra (T = Si, Al), where the AlO_4^- tetrahedra are charge-balanced by Na^+ ions, located at the center of 6R and 8R (6- and 8-membered rings) [55–57]. Within the fundamental unit cell (β cage), interference in atomic positions and density are primarily responsible for changes in peak intensities. Due to the differences in the ionic radius of Cs^+ (3.6 Å) and Na^+ (1.24 Å), $Cs^+ \leftrightarrow Na^+$ exchanges take place at the center of 8R (8-membered rings), due to the appropriate fitting of Cs^+ into the ring cavity (3.6 – 4.1 Å in diameter) [33,58,59]. Literature reports that Cs selectivity in zeolites (Si/Al: 1 – 2) has been shown to range from 72 – 98% in structures that contain 8R, while this value is 40 – 60% in those without 8R [10,59]. The pattern of the ZeoACs sample exhibits changes in the intensity of peaks related to different crystal orientations, such as 100, 111, 321, 410, and others, as a result of the $Cs^+ \leftrightarrow Na^+$ exchange. These changes suggest that the selectivity of Cs in the zeolite sample derived from this specific CFA is high. Analyzing the SEM images shown in Figure. 2, which correspond to the raw zeolite A (a,b) and the Cs-loaded zeolite (c,d), it can be observed that the high crystallinity and phase purity of the ash-derived zeolite, previously suggested by the XRD pattern (Figure. 1), are reflected in the morphology, which features homogenously distributed, sharp-edged cubic particles with no visible point defects. It is known that highly crystalline zeolites exhibit excellent ionic selectivity due to the regular size of pores and rings, creating three-dimensional tunnels that facilitate the transport of hydrated ions in aqueous solutions [60]. Zeolite particles are often interconnected as clusters, and crystal growth can occur in more than one direction. However, the growth mechanism is not completely understood for a given system, due to the multiple variables involved, such as the nature of the aluminum source and potential organic contaminants, which are known to favor cubic particles with chamfered edges [61,62].

When comparing the FTIR spectral groups before (raw) and after (ZeoACs) the sorption experiment, shown in Figure. 3, it is observed that the partial exchange of Na^+ for Cs^+ in the zeolite does not alter any peak or band in the analyzed range (400 – 4000 cm^{-1}), except for the shift from 3420 cm^{-1} to 3444 cm^{-1}. This shift occurs due to the greater interaction of Cs^+ ions with the OH functional groups of adsorbed water molecules, when compared to Na^+ [33]. The framework structure of the zeolitic material is shown to be maintained after the sorption experiment, a fact that is also favored by the experimental conditions, such as room temperature, stable pH, and the absence of competitive ions in the simulated CsCl solution [63].

Raman scattering is useful in revealing specific structural units present in both amorphous and crystalline states. When analyzing the Raman spectra collected on the zeolite A before and after the sorption experiment, shown in Figure. 4, it is observed that, similarly to the infrared transmittance (Figure. 3), the material did not exhibit shifts in Raman band positions. Instead, only increased frequencies were observed for the bands at 281 cm^{-1} and 338 cm^{-1}, indicating that cesium does not interfere with the vibrations of 4-membered rings [64]. The relationship between the Raman bands in the region from 300 cm^{-1} to 600 cm^{-1} and the size of structural rings in crystalline silicate and aluminosilicate materials, such as zeolites, is reported in the literature [45–49]. The smaller the size of the rings, the higher the vibration frequency of these structures. Therefore, the band at 281 cm^{-1} is related to the vibrational bending mode of rings containing more than 4 or 6 members, in this case, the 8-membered ring of zeolite A. These rings make up the pores with a diameter of 4.2 Å, which give access to the central supercavity (11.4 Å) of its crystalline structure [45–49,64]. Such alterations are due to an interference in the bending vibrational mode of 8- and 6-membered rings, respectively, caused by the difference between the ionic radii of Cs^+ and Na^+ [33,64].

From the data in Table 3, it is observed that the zeolite sample was able to retain 0.26 g of Cs per gram of zeolite (26 wt.%) through the exchange of Na^+ for Cs^+. Although the exchangeable sites of this zeolitic material are not fully charge-balanced by Na^+, but rather contain other cations, the differences in exchange capacity and hydrated ionic sizes of Ca^{2+}, Fe^{3+}, Ti^{2+}, and other minor constituents were overcome by the good retention of Cs [46,47,49,65]. Additionally, it is known from the literature that factors such as contact time, the amount of zeolitic material, the concentration of Cs in the solution, and particle size may influence the adsorption efficiency in this type of experiment [66]. The ash-derived zeolite produced in this work thus exhibits adequate Cs adsorption due to its homogeneous morphology and structural characteristics.

Since this type of waste form is commonly used in thermal processes for vitrification, the thermal behavior of the Cs-loaded zeolite A during heating up to 1000 °C was evaluated through differential and thermogravimetric analyses, as shown in Figure. 5. During heating, the ZeoACs sample exhibits endothermic deviations in the DTA curve, indicating that energy is being consumed for the evaporation of adsorbed water molecules [67,68]. This event reaches its maximum at 96.99 °C, shown by a substantial mass loss of about 6.3%. As the temperature increases, the zeolite exhibits an exothermic deviation (DTA), and up to 400 °C, the mass loss reaches 11.46%, suggesting that much of the decarbonation has already occurred, as the rate of mass loss relatively stabilizes (DTG) [67]. However, at 700 °C, a pronounced exothermic deviation is observed (DTA) with a maximum around 850 °C, indicating the structural collapse of the zeolitic framework. At this stage, there is an additional mass loss of 2.39% at 874.82 °C, suggesting the desorption of remaining organic material [69]. Finally, at 960 °C, an endothermic peak is observed (DTA), suggesting a transformation of the material into new crystalline phase(s), which will be evaluated.

In Figure. 6, the stability of Cs is observed through the thermal evolution of its crystalline phases, as the material undergoes

structural collapse and the first crystalline nuclei begin to form simultaneously. This is shown by the XRD pattern of the sample heat-treated at 845 ºC, which was previously represented by the amorphous exothermic DTA deviation (Figure. 5). Interestingly, the crystalline phases involving Cs exhibit good stability with increasing temperature and consolidate around 960 ºC, consistent with the exothermic peak, which reaches its maximum at this temperature, as shown in the DTA result (Figure. 5). The Na-A zeolite produced from the coal fly ash used in this work demonstrates itself to be a safe adsorbent material for the decontamination of cesium-137 from liquid nuclear wastes, because Cs atoms are thermally immobilized in water-insoluble phases of pollucite and cesium aluminum oxide [70].

Factors such as the specific surface area and porosity of this zeolite-based waste form are particularly important when considering potential contact with groundwater. This is why zeolitic materials are commonly used as adsorbents in an intermediate step of nuclear waste immobilization and are often incorporated into high-density matrices, such as glasses and geopolymers [69,71].

Since the chemical resistance of the specimens is governed by the specific area in contact with water, the surface was evaluated, and the results are shown in Figure. 7 by the SEM micrographs. In Figure. 7 (column a), it is observed that the ZeoACs sample exhibits a rough surface containing deep microcracks and heterogeneous morphology, which suggests that the thermal energy supplied up to 900 °C is not sufficient to obtain a dense monolithic material. When plotting the zeolite composition into the ternary phase diagram: $47SiO_2$-$40Al_2O_3$-$13Na_2O$, the composition lies in the crystallization field of mullite, and the liquidus projection reveals that the material melts at around 1680°C [72]. This indicates that, even though the heating temperature (900 °C) was higher than half of the melting point (840°C), it was not sufficient for densification. Zeolites are extremely porous materials, meaning that heat transfer cannot occur solely by atom-to-atom transmission, as it does for bulk materials, but also competes with the structural discontinuities represented by the surface area and the structural channels [9,60].

However, when examining the micrographs shown in Figure. 7 (column b), it is observed that the G6ZCs sample presents a dense surface without microcracks and very few pores, indicating that the mixture of glass particles with the ZeoACs zeolite is more effective in the densification of the waste form, improving the coalescence kinetics [73,74]. The existence of the crystalline phases previously detected in the ZeoACs sample is also indicated (column a) by the presence of dense, round, large particles distributed in a matrix of homogeneously small, interconnected particles. Similarly, different-sized and shaped particles can be seen in the dense G6ZCs sample (column b), suggesting the existence of several crystalline phases, as expected, due to the complex composition of the material resulting from the mixture of Nb-aluminoborosilicate glass and ZeoACs.

From the data contained in Table 4, it can be inferred that the immobilization of Cs using Nb-aluminoborosilicate glass matrices is an interesting process because the Cs content previously incorporated into the zeolite was proportionally maintained in the G6ZCs sample (3:2 wt. fraction), meaning no volatilization occurred up to 900 °C. Also, from the data obtained by the ASTM C373-88 standard test [40] on the heat-treated samples (900 ºC/2h), it is observed that the G6ZCs sample exhibited a higher density (2.4 g/cm^3) than the ZeoACs sample (1.44 g/cm^3). As a result, the water absorption is low for G6ZCs (1.63 wt.%) and high for ZeoACs (33.4 wt.%). The water absorption of a ceramic body is directly associated with the specific surface area in contact with water, including defects such as pores and microcracks, which accelerate the leaching of immobilized species [75,76]. The porosity of the G6ZCs sample consists mostly of impervious regions, rather than open pores, whereas for the ZeoACs sample, the porosity is equally distributed between both types of pores, which is unsuitable for long-term disposal due to the potential for leaching by groundwater. Although Nb-aluminoborosilicate glasses showed higher resistance to crystallization in our previous work [27], when mixed with zeolitic materials, which are aluminosilicate crystalline materials, factors such as the compositional increase in Si and Al were shown to alter the overall composition and thermodynamics of the phases [27,76].

Another excellent option for the selective immobilization of Cs is the incorporation of Cs-loaded zeolites into geopolymer matrices. The leaching of Cs in geopolymers is usually lower than in concrete, due to differences in porosity [17,52–54]. The leaching rate (LR) and cumulative fraction leached of the ZG specimen (Cs-loaded zeolite + geopolymer matrix) are shown in Figure. 8 (a,b). It is observed that the initial leaching rate of the ZG specimens on day 1 is around $4.5x10^{-6}$ $cm.d^{-1}$, reaching a maximum on day 2 ($5.8x10^{-6}$ $cm.d^{-1}$). However, there is a substantial decrease on day 3, which continues throughout the subsequent days, showing stability with $1.23x10^{-6}$ $cm.d^{-1}$ on day 11. This trend is reflected in the cumulative fraction leached. It is known from the literature that geopolymer solidified blocks present higher leaching resistance to Sr^{2+} and Cs^+ (10^{-4} to 10^{-6} $g{\cdot}cm^{-2}{\cdot}d^{-1}$) than cement ($10^{-3}$ to 10^{-4} $g{\cdot}cm^{-2}{\cdot}d^{-1}$), in deionized water and other media such as acetic acid solutions (pH = 3.6), magnesium sulfate solutions ($MgSO_4$ = 5 wt.%), and sulfuric acid solutions (pH = 1) [38]. Comparing the leaching behavior of similar geopolymer samples found in the literature (around $1x10^{-2}$ $cm.d^{-1}$), it can be concluded that ZG specimens are well-suited for the immobilization of radioactive cesium using Cs-loaded ash-derived zeolite A [17,38,51–54].

5. CONCLUSION

Highly phase-pure zeolite A was synthesized via a hydrothermal process using fly ash from a coal-based thermal power plant in Brazil and loaded with Cs for evaluation of thermal stability, structure, and immobilization in Nb-aluminoborosilicate and geopolymer matrices. The exchange of Na^+ for Cs^+ was evaluated through changes in the intensity of XRD peaks and in the Raman bands related to 6- and 8-membered structural rings, compared to the raw zeolite, confirming good Cs adsorption. A total of 26 wt.% of Cs was incorporated (INAA) after the sorption experiments conducted for 24 hours using a simulated (non-radioactive) CsCl solution, which is a notable result for a zeolite synthesized from coal fly ash, considering its inherent impurities. The retention of Cs in the microstructure of the zeolitic material remained stable up to 960 °C, with the presence of two water-insoluble phases, pollucite and cesium aluminum oxide, even though the zeolitic material undergoes substantial structural collapse during the heating process (700 °C – 900 °C). Up to 40 wt.% of the simulated

nuclear waste material with the quantities defined by Equation 1, after the initial wash-off period, a rapid increase in the leaching of cesium attached to the surface of the ZG specimens is observed. The LR is primarily controlled by diffusion in a steady-state mode at a constant rate. The LR calculated for the 11th leaching day was 1.23×10-2 cm.d-1. This result is in good agreement with those reported in the literature [17,38,51–54]. could be incorporated into a monolithic dense ceramic body obtained through the heat-induced densification process on uniaxially pressed mixtures of Nb-aluminoborosilicate powder glass and Cs-loaded zeolite A. By applying 900 °C for 2 hours, bulk densities around 2.4 g/cm^3 were obtained, resulting in very low apparent porosity (3.6%) and low water absorption (1.63%) for the G6ZCs specimen, whereas the raw Cs-loaded zeolite A (ZeoACs) exhibited the highest porosity (48%), water absorption (33%), and the lowest density (1.44 g/cm^3). The growth of crystalline phases involving Cs at a lower temperature (up to 900 °C) compared to the raw Cs-loaded zeolite (960 °C) was made possible by the use of Nb-aluminoborosilicate glass due to its natural crystallization during heating. When applying the ash-derived zeolite for the immobilization of the radioactive tracer (^{137}Cs) into geopolymer matrices, the Cs leachability under water was compatible with materials found in the literature, confirming that the obtained waste forms meet the requirements for nuclear waste disposal.with similar materials found in the literature, confirming that the obtained waste forms meet the requirements for nuclear waste disposal.

ACKNOWLEDGEMENTS

This work was supported by the Nuclear and Energy Research Institute (IPEN/USP) (project n. 2018.05.IPEN.14).

CREDIT AUTHOR STATEMENT

Mello-Castanho, S: Supervision, Conceptualization, Methodology, Writing-Reviewing and Editing. Costa-Silva, D. L: Investigation, Data curation, Formal analysis, Writing-Original draft preparation and Editing. Fungaro, D. A: Visualization, Data curation, Formal analysis. Las Casas, A: Data curation, Writing-Reviewing and Editing. Silva, P. S. C: Data curation, Formal analysis. Vicente, R: Data curation, Formal analysis. Araujo, M. S: Conceptualization, Methodology. Izidoro, J. C: Methodology, Formal analysis.

DECLARATIONS

Conflict of interest The authors declare that they have no known competing financial interests or personal relationships that could have appeared to influence the work reported in this paper.

REFERENCES

[1] S. Shimizutani, H. Yamada, Long-term consequences of the atomic bombing in Hiroshima, J Jpn Int Econ 59 (2021) 101119. https://doi.org/10.1016/J.JJIE.2020.101119.

[2] M. Tomonaga, The Atomic Bombings of Hiroshima and Nagasaki: A Summary of the Human Consequences, 1945-2018, and Lessons for Homo sapiens to End the Nuclear Weapon Age, Journal for Peace and Nuclear Disarmament 2 (2019) 491–517. https://doi.org/10.1080/25751654.2019.1681226.

[3] G. Rothwell, Spent nuclear fuel storage: What are the relationships between size and cost of the alternatives?, Energy Policy 150 (2021) 112126. https://doi.org/10.1016/J.ENPOL.2020.112126.

[4] I. Ruuska, K. Artto, K. Aaltonen, P. Lehtonen, Dimensions of distance in a project network: Exploring Olkiluoto 3 nuclear power plant project, International Journal of Project Management 27 (2009) 142–153. https://doi.org/10.1016/J.IJPROMAN.2008.09.003.

[5] M.I. Ojovan, S. V. Yudintsev, Glass, ceramic, and glass-crystalline matrices for HLW immobilisation, Open Ceramics 14 (2023) 100355. https://doi.org/10.1016/j.oceram.2023.100355.

[6] M.I. Ojovan, W.E. Lee, S.N. Kalmykov, Immobilisation of Radioactive Wastes in Glass, An Introduction to Nuclear Waste Immobilisation (2019) 319–368. https://doi.org/10.1016/B978-0-08-102702-8.00019-4.

[7] T.J. Yasunari, A. Stohl, R.S. Hayano, J.F. Burkhart, S. Eckhardt, T. Yasunari, Cesium-137 deposition and contamination of Japanese soils due to the Fukushima nuclear accident, Proceedings of the National Academy of Sciences 108 (2011) 19530–19534. https://doi.org/10.1073/pnas.1112058108.

[8] S. Khandaker, Y. Toyohara, S. Kamida, T. Kuba, Effective removal of cesium from wastewater solutions using an innovative low-cost adsorbent developed from sewage sludge molten slag, J Environ Manage 222 (2018) 304–315. https://doi.org/10.1016/j.jenvman.2018.05.059.

[9] H.N. Yeritsyan, A.A. Sahakyan, V. V. Harutunyan, S.K. Nikoghosyan, E.A. Hakhverdyan, N.E. Grigoryan, Natural zeolites and application in liquid waste treatment, in: Brilliant Light in Life and Material Sciences, Springer Netherlands, Dordrecht, n.d.: pp. 395–401. https://doi.org/10.1007/978-1-4020-5724-3_38.

[10] M. Jiménez-Reyes, P.T. Almazán-Sánchez, M. Solache-Ríos, Radioactive waste treatments by using zeolites. A short review, J Environ Radioact 233 (2021) 106610. https://doi.org/10.1016/j.jenvrad.2021.106610.

[11] I. Smičiklas, I. Coha, M. Jović, M. Nodilo, M. Šljivić-Ivanović, S. Smiljanić, Ž. Grahek, Efficient separation of strontium radionuclides from high-salinity wastewater by zeolite 4A synthesized from Bayer process liquids, Sci Rep 11 (2021) 1738. https://doi.org/10.1038/s41598-021-81255-y.

[12] X.-H. Fang, F. Fang, C.-H. Lu, L. Zheng, Removal of Cs+, Sr2+, and Co2+ Ions from the Mixture of Organics and Suspended Solids Aqueous Solutions by Zeolites, Nuclear Engineering and Technology 49 (2017) 556–561. https://doi.org/10.1016/j.net.2016.11.008.

[13] M.W. Munthali, E. Johan, H. Aono, N. Matsue, Cs + and Sr 2+ adsorption selectivity of zeolites in relation to radioactive decontamination, Journal of Asian Ceramic Societies 3 (2015) 245–250. https://doi.org/10.1016/j.jascer.2015.04.002.

[14] S.T. Reis, J.R. Martinelli, Cs immobilization by sintered lead iron phosphate glasses, J Non Cryst Solids 247 (1999). https://doi.org/10.1016/S0022-3093(99)00078-2.

[15] C.W. Kim, D.E. Day, Immobilization of Hanford LAW in iron phosphate glasses, J Non Cryst Solids 331 (2003). https://doi.org/10.1016/j.jnoncrysol.2003.08.070.
[16] J.S. McCloy, A. Goel, Glass-ceramics for nuclear-waste immobilization, MRS Bull 42 (2017) 233–240. https://doi.org/DOI: 10.1557/mrs.2017.8.
[17] Q. Li, Z. Sun, D. Tao, Y. Xu, P. Li, H. Cui, J. Zhai, Immobilization of simulated radionuclide 133Cs+ by fly ash-based geopolymer, J Hazard Mater 262 (2013) 325–331. https://doi.org/10.1016/j.jhazmat.2013.08.049.
[18] C.L. Thorpe, J.J. Neeway, C.I. Pearce, R.J. Hand, A.J. Fisher, S.A. Walling, N.C. Hyatt, A.A. Kruger, M. Schweiger, D.S. Kosson, C.L. Arendt, J. Marcial, C.L. Corkhill, Forty years of durability assessment of nuclear waste glass by standard methods, Npj Mater Degrad 5 (2021) 61. https://doi.org/10.1038/s41529-021-00210-4.
[19] Werner. Lutze, R.C. Ewing, Radioactive waste forms for the future, North-Holland, 1988. https://inis.iaea.org/search/search.aspx?orig_q=RN:20061516 (accessed January 4, 2024).
[20] C.M. Jantzen, Nuclear Waste Glass Durability: I, Predicting Environmental Response from Thermodynamic (Pourbaix) Diagrams, Journal of the American Ceramic Society 75 (1992) 2433–2448. https://doi.org/10.1111/j.1151-2916.1992.tb05596.x.
[21] E. Boué, S. Schuller, M.J. Toplis, T. Charpentier, A. Mesbah, H. Pablo, M. Monnereau, M. Moskura, Kinetic and thermodynamic factors controlling the dissolution of molybdate-bearing calcines during nuclear glass synthesis, Journal of Nuclear Materials 519 (2019) 74–87. https://doi.org/10.1016/j.jnucmat.2019.03.037.
[22] S. Pangdaeng, V. Sata, J.B. Aguiar, F. Pacheco-Torgal, J. Chindaprasirt, P. Chindaprasirt, Bioactivity enhancement of calcined kaolin geopolymer with CaCl2 treatment, ScienceAsia 42 (2016) 407. https://doi.org/10.2306/scienceasia1513-1874.2016.42.407.
[23] J. Davidovits, Geopolymer Chemistry and Applications, 2008.
[24] P. Adamiec, J.-C. Benezet, A. Benhassaine, Pozzolanic reactivity of silico-aluminous fly ash, Particuology 6 (2008) 93–98. https://doi.org/10.1016/j.partic.2007.09.003.
[25] P. Lichvar, M. Rozloznik, S. Sekely, Behaviour of Aluminosilicate Inorganic Matrix SIAL During and After Solidification of Radioactive Sludge and Radioactive Spent Resins and Their Mixtures, 2013.
[26] D.B. Istuque, L. Soriano, J.L. Akasaki, J.L.P. Melges, M.V. Borrachero, J. Monzó, J. Payá, M.M. Tashima, Effect of sewage sludge ash on mechanical and microstructural properties of geopolymers based on metakaolin, Constr Build Mater 203 (2019) 95–103. https://doi.org/10.1016/j.conbuildmat.2019.01.093.
[27] D.L. Costa-silva, J.F. Bartolomé, A.C. Silva, S. Mello-Castanho, Structural and thermal influence of niobia in aluminoborosilicate glasses, Ceram Int 48 (2022) 18433–18440. https://doi.org/10.1016/j.ceramint.2022.03.112.
[28] Z.T. Yao, X.S. Ji, P.K. Sarker, J.H. Tang, L.Q. Ge, M.S. Xia, Y.Q. Xi, A comprehensive review on the applications of coal fly ash, Earth Sci Rev 141 (2015) 105–121. https://doi.org/10.1016/j.earscirev.2014.11.016.
[29] A. Shoumkova, V. Stoyanova, Zeolites formation by hydrothermal alkali activation of coal fly ash from thermal power station "Maritsa 3", Bulgaria, Fuel 103 (2013) 533–541. https://doi.org/10.1016/j.fuel.2012.07.076.
[30] J. Izidoro, D. Castanho, C. Rossati, D. Fungaro, S. Guilhen, T. Nogueira, M. De Fátima Andrade, Application of high-purity zeolite a synthesized from different coal combustion by-products in carbon dioxide capture, International Journal of Environmental Impacts: Management, Mitigation and Recovery 2 (2019) 215–228. https://doi.org/10.2495/EI-V2-N3-215-228.
[31] J. de C. Izidoro, D.A. Fungaro, F.S. dos Santos, S. Wang, Characteristics of Brazilian coal fly ashes and their synthesized zeolites, Fuel Processing Technology 97 (2012) 38–44. https://doi.org/10.1016/j.fuproc.2012.01.009.
[32] A. Bhatt, S. Priyadarshini, A. Acharath Mohanakrishnan, A. Abri, M. Sattler, S. Techapaphawit, Physical, chemical, and geotechnical properties of coal fly ash: A global review, Case Studies in Construction Materials 11 (2019) e00263. https://doi.org/10.1016/j.cscm.2019.e00263.
[33] Q. Tian, K. Sasaki, Application of fly ash-based materials for stabilization/solidification of cesium and strontium, Environmental Science and Pollution Research 26 (2019) 23542–23554. https://doi.org/10.1007/s11356-019-05612-1.
[34] A.C. Silva, S. Mello-Castanho, F. Guitian, I. Montero, A. Esteban-Cubillo, I. Sobrados, J. Sanz, J.S. Moya, Incorporation of galvanic waste (Cr, Ni, Cu, Zn, Pb) in a soda-lime-borosilicate glass, Journal of the American Ceramic Society 91 (2008). https://doi.org/10.1111/j.1551-2916.2008.02311.x.
[35] A.C. Silva, S.R.H. Mello-Castanho, Vitrified galvanic waste chemical stability, J Eur Ceram Soc 27 (2007). https://doi.org/10.1016/j.jeurceramsoc.2006.04.110.
[36] D.L. Costa-Silva, M.S. Araujo, D.A. Fungaro, P.S.C. Silva, S. Mello-Castanho, New approach to niobia-modified borosilicate glasses for Cs waste immobilization, Journal of Materials Research and Technology 31 (2024) 1229–1235. https://doi.org/10.1016/j.jmrt.2024.06.099.
[37] ASTM C1308-21, Standard test method for accelerated leach test for measuring contaminant releases from solidified waste, ASTM International, West Conshohocken, PA i (2021).org/10.1016/j.net.2016.11.008.
[38] Z. Xu, Z. Jiang, D. Wu, X. Peng, Y. Xu, N. Li, Y. Qi, P. Li, Immobilization of strontium-loaded zeolite A by metakaolin based-geopolymer, Ceram Int 43 (2017) 4434–4439. https://doi.org/10.1016/j.ceramint.2016.12.092.
[39] K. Momma, F. Izumi, VESTA 3 for three-dimensional visualization of crystal, volumetric and morphology data, J Appl Crystallogr 44 (2011). https://doi.org/10.1107/S0021889811038970.
[40] W.C.P. ASTM International, ASTM 1285-02 Standard test method for water absorption, bulk density, apparent density, and apparent specific gravity of fired whitewares products., 2002.
[41] R.W. Stevens, R. V. Siriwardane, J. Logan, In Situ Fourier Transform Infrared (FTIR) Investigation of CO2 Adsorption onto Zeolite Materials, Energy & Fuels 22 (2008)

3070–3079. https://doi.org/10.1021/ef800209a.
[42] S. Markovic, V. Dondur, R. Dimitrijevic, FTIR spectroscopy of framework aluminosilicate structures: carnegieite and pure sodium nepheline, J Mol Struct 654 (2003) 223–234. https://doi.org/10.1016/S0022-2860(03)00249-7.
[43] S.S. Rayalu, J.S. Udhoji, S.U. Meshram, R.R. Naidu, S. Devotta, Estimation of crystallinity in flyash-based zeolite-A using XRD and IR spectroscopy, Curr Sci 89 (2005) 2147–2151. http://www.jstor.org/stable/24111077.
[44] X. Ren, L. Xiao, R. Qu, S. Liu, D. Ye, H. Song, W. Wu, C. Zheng, X. Wu, X. Gao, Synthesis and characterization of a single phase zeolite A using coal fly ash, RSC Adv 8 (2018) 42200–42209. https://doi.org/10.1039/C8RA09215J.
[45] T. Wang, S. Luo, G.A. Tompsett, M.T. Timko, W. Fan, S.M. Auerbach, Critical Role of Tricyclic Bridges Including Neighboring Rings for Understanding Raman Spectra of Zeolites, J Am Chem Soc 141 (2019) 20318–20324. https://doi.org/10.1021/jacs.9b10346.
[46] P.K. Dutta, D.C. Shieh, Crystallization of zeolite A: a spectroscopic study, J Phys Chem 90 (1986) 2331–2334. https://doi.org/10.1021/j100402a017.
[47] P.K. Dutta, B. Del Barco, Raman spectroscopy of zeolite A: influence of silicon/aluminum ratio, J Phys Chem 92 (1988) 354–357. https://doi.org/10.1021/j100313a022.
[48] T.F. Chaves, F.L.F. Soares, D. Cardoso, R.L. Carneiro, Monitoring of the crystallization of zeolite LTA using Raman and chemometric tools, Analyst 140 (2015) 854–859. https://doi.org/10.1039/C4AN00913D.
[49] Y. Yu, G. Xiong, C. Li, F.-S. Xiao, Characterization of aluminosilicate zeolites by UV Raman spectroscopy, Microporous and Mesoporous Materials 46 (2001) 23–34. https://doi.org/10.1016/S1387-1811(01)00271-2.
[50] C.J. Rhodes, T.C. Dintinger, Radiation Effects on Zeolite Nanomaterials - Some Potential Implications for Cleaning Liquid Nuclear Waste and for Enhanced Radioactive Decontamination, Progress in Reaction Kinetics and Mechanism 37 (2012) 103–137. https://doi.org/10.3184/146867812X13323521255195.
[51] J.L. Provis, J.S.J. Van Deventer, 1 - Introduction to geopolymers, in: J.L. Provis, J.S.J. van Deventer (Eds.), Geopolymers, Woodhead Publishing, 2009: pp. 1–11. https://doi.org/https://doi.org/10.1533/9781845696382.1.
[52] R. Abdelrahman, A. Zaki, A. Elkamash, Modeling the long-term leaching behavior of 137Cs, 60Co, and 152,154Eu radionuclides from cement–clay matrices, J Hazard Mater 145 (2007) 372–380. https://doi.org/10.1016/j.jhazmat.2006.11.030.
[53] I. Tsuneki, W. Sadayuki, A. Hiroyuki, H. Kazuko, Y. Kazuo, Metakaolin-based Geopolymer for Immobilizing Concentrated Cs Generated by Volume Reduction of 137 Cs-contaminated Waste, in: 2020. https://api.semanticscholar.org/CorpusID:221803897.
[54] S. Jain, N. Banthia, T. Troczynski, Leaching of immobilized cesium from NaOH-activated fly ash-based geopolymers, Cem Concr Compos 133 (2022) 104679. https://doi.org/10.1016/j.cemconcomp.2022.104679.
[55] K. Ooe, T. Seki, K. Yoshida, Y. Kohno, Y. Ikuhara, N. Shibata, Direct imaging of local atomic structures in zeolite using novel low-dose scanning transmission electron microscopy, in: 2023. https://api.semanticscholar.org/CorpusID:255595946.
[56] Z. Dong, E. Zhang, Y. Jiang, Q. Zhang, A. Mayoral, H. Jiang, Y. Ma, Atomic-Level Imaging of Zeolite Local Structures Using Electron Ptychography, J Am Chem Soc 145 (2023) 6628–6632. https://doi.org/10.1021/jacs.2c12673.
[57] V. Psycharis, V. Perdikatsis, G. Christidis, Crystal structure and rietveld refinement of zeolite a synthesized from fine-grained perlite waste materials, Bulletin of the Geological Society of Greece 36 (2004) 121. https://doi.org/10.12681/bgsg.16591.
[58] M. Mahima Kumar, K.A. Irshad, H. Jena, Removal of Cs+ and Sr2+ ions from simulated radioactive waste solutions using Zeolite-A synthesized from kaolin and their structural stability at high pressures, Microporous and Mesoporous Materials 312 (2021) 110773. https://doi.org/10.1016/j.micromeso.2020.110773.
[59] S. Kwon, C. Kim, E. Han, H. Lee, H.S. Cho, M. Choi, Relationship between zeolite structure and capture capability for radioactive cesium and strontium, J Hazard Mater 408 (2021) 124419. https://doi.org/10.1016/j.jhazmat.2020.124419.
[60] M. Kuronen, M. Weller, R. Townsend, R. Harjula, Ion exchange selectivity and structural changes in highly aluminous zeolites, React Funct Polym 66 (2006) 1350–1361. https://doi.org/10.1016/j.reactfunctpolym.2006.03.019.
[61] J. Grand, H. Awala, S. Mintova, Mechanism of zeolites crystal growth: new findings and open questions, CrystEngComm 18 (2016) 650–664. https://doi.org/10.1039/C5CE02286J.
[62] B.C. Amoni, A.D.L. Freitas, R.A. Bessa, C.P. Oliveira, M. Bastos-Neto, D.C.S. Azevedo, S.M.P. Lucena, J.M. Sasaki, J.B. Soares, S.A. Soares, A.R. Loiola, Effect of coal fly ash treatments on synthesis of high-quality zeolite A as a potential additive for warm mix asphalt, Mater Chem Phys 275 (2022) 125197. https://doi.org/10.1016/J.MATCHEMPHYS.2021.125197.
[63] I. Dianellou, F. Karantoumanis, P. Tsamos, F. Noli, The effect of irradiation on the Cs, Co and Eu-removal from aqueous solutions using Greek minerals, J Radioanal Nucl Chem 332 (2023). https://doi.org/10.1007/s10967-023-08857-w.
[64] K. Yoshida, K. Toyoura, K. Matsunaga, A. Nakahira, H. Kurata, Y.H. Ikuhara, Y. Sasaki, Atomic sites and stability of Cs+ captured within zeolitic nanocavities, Sci Rep 3 (2013) 2457. https://doi.org/10.1038/srep02457.
[65] M. Omerašević, M. Lukić, M. Savić-Biserčić, A. Savić, L. Matović, Z. Baščarević, D. Bučevac, Permanent disposal of Cs ions in the form of dense pollucite ceramics having low thermal expansion coefficient, Nuclear Engineering and Technology 52 (2020) 115–122. https://doi.org/10.1016/j.net.2019.07.001.
[66] M. Şenilă, E. Neag, C. Tănăselia, L. Şenilă, Removal of Cesium and Strontium Ions from Aqueous Solutions by Thermally Treated Natural Zeolite, Materials 16 (2023). https://doi.org/10.3390/ma16082965.
[67] M.K. Król, P. Jeleń, The Effect of Heat Treatment on the Structure of Zeolite A, Materials 14 (2021) 4642. https://doi.org/10.3390/ma14164642.

[68] H. Mimura, M. Saito, K. Akiba, Y. Onodera, Selective Uptake of Cesium by Ammonium Molybdophosphate (AMP)-Calcium Alginate Composites, J Nucl Sci Technol 38 (2001) 872–878. https://doi.org/10.1080/18811248.2001.9715108.
[69] S. Komarneni, R. Roy, Zeolites for fixation of cesium and strontium from radwastes by thermal and hydrothermal treatments, Nuclear and Chemical Waste Management 2 (1981) 259–264. https://doi.org/10.1016/0191-815X(81)90052-8.
[70] Y. Yokomori, K. Asazuki, N. Kamiya, Y. Yano, K. Akamatsu, T. Toda, A. Aruga, Y. Kaneo, S. Matsuoka, K. Nishi, S. Matsumoto, Final storage of radioactive cesium by pollucite hydrothermal synthesis, Sci Rep 4 (2014) 4195. https://doi.org/10.1038/srep04195.
[71] H. Kazemian, P. Darybi-Kasmaei, M.H. Mallah, M.R. Khani, Vitrification of Cs and Sr loaded Iranian natural and synthetic zeolites, J Radioanal Nucl Chem 267 (2005) 219–223. https://doi.org/10.1007/s10967-006-0030-z.
[72] Robert S. Roth, Taki Negas, Lawrence P. Cook, Phase Diagrams for Ceramists, ACERS, American Ceramic Society, 1981.
[73] F. Matteucci, M. Dondi, G. Guarini, Effect of soda-lime glass on sintering and technological properties of porcelain stoneware tiles, Ceram Int 28 (2002) 873–880. https://doi.org/10.1016/S0272-8842(02)00067-6.
[74] B. Hoghooghi, J. McKittrick, C. Butler, P. Desch, Synthesis of celsian ceramics from zeolite precursors, J Non Cryst Solids 170 (1994) 303–307. https://doi.org/10.1016/0022-3093(94)90061-2.
[75] J. Dávalos, A. Bonilla, M.A. Villaquirán-Caicedo, R.M. de Gutiérrez, J.Ma. Rincón, Preparation of glass–ceramic materials from coal ash and rice husk ash: Microstructural, physical and mechanical properties, Boletín de La Sociedad Española de Cerámica y Vidrio 60 (2021) 183–193. https://doi.org/10.1016/j.bsecv.2020.02.002.
[76] A. Goel, J.S. McCloy, K.M. Fox, C.J. Leslie, B.J. Riley, C.P. Rodriguez, M.J. Schweiger, Structural analysis of some sodium and alumina rich high-level nuclear waste glasses, J Non Cryst Solids 358 (2012) 674–679. https://doi.org/10.1016/J.JNONCRYSOL.2011.11.015.
[71] H. Kazemian, P. Darybi-Kasmaei, M.H. Mallah, M.R. Khani, Vitrification of Cs and Sr loaded Iranian natural and synthetic zeolites, J Radioanal Nucl Chem 267 (2005) 219–223. https://doi.org/10.1007/s10967-006-0030-z.
[72] Robert S. Roth, Taki Negas, Lawrence P. Cook, Phase Diagrams for Ceramists, ACERS, American Ceramic Society, 1981.
[73] F. Matteucci, M. Dondi, G. Guarini, Effect of soda-lime glass on sintering and technological properties of porcelain stoneware tiles, Ceram Int 28 (2002) 873–880. https://doi.org/10.1016/S0272-8842(02)00067-6.
[74] B. Hoghooghi, J. McKittrick, C. Butler, P. Desch, Synthesis of celsian ceramics from zeolite precursors, J Non Cryst Solids 170 (1994) 303–307. https://doi.org/10.1016/0022-3093(94)90061-2.
[75] J. Dávalos, A. Bonilla, M.A. Villaquirán-Caicedo, R.M. de Gutiérrez, J.Ma. Rincón, Preparation of glass–ceramic materials from coal ash and rice husk ash: Microstructural, physical and mechanical properties, Boletín de La Sociedad Española de Cerámica y Vidrio 60 (2021) 183–193. https://doi.org/10.1016/j.bsecv.2020.02.002.
[76] A. Goel, J.S. McCloy, K.M. Fox, C.J. Leslie, B.J. Riley, C.P. Rodriguez, M.J. Schweiger, Structural analysis of some sodium and alumina rich high-level nuclear waste glasses, J Non Cryst Solids 358 (2012) 674–679. https://doi.org/10.1016/J.JNONCRYSOL.2011.11.015.